Environmental Science Processes & Impacts

# Towards a Comprehensive Understanding of Malathion Degradation: Theoretical Investigation of Degradation Pathways and Related Kinetics under Alkaline Conditions



| | |
|---|---|
| Journal: | *Environmental Science: Processes & Impacts* |
| Manuscript ID | EM-ART-05-2021-000181.R1 |
| Article Type: | Paper |
| | |

Malathion is a commercial organophosphate insecticide which functions as an acetylcholinesterase inhibitor. Both this organophosphate moiety and its mechanism of action are common across a variety of pesticide compounds. Research has previously shown how malathion degrades in the environment. However, there is limited study on subsequent degradation of the initial breakdown products. Our computational data demonstrate that the initial products can, in several cases, continue to degrade into species that may continue to pose a threat to terrestrial and aquatic life if left unconsidered in the broader picture of toxicity and remediation. These implications of these reactions can potentially be extrapolated to structurally similar organophosphorus compounds.

# Towards a Comprehensive Understanding of Malathion Degradation: Theoretical Investigation of Degradation Pathways and Related Kinetics under Alkaline Conditions

*Robert W. Lamb[1,2], Harley McAlexander[2], Christa M. Woodley[2], and Manoj K. Shukla[2]**

[1]Oak Ridge Institute for Science and Education, Oak Ridge, TN, USA

[2]US Army Engineer Research and Development Center, Environmental Laboratory, 3909 Halls Ferry Road, Vicksburg, MS 39180, USA

ABSTRACT

Malathion is a commercially available insecticide that functions by acting as an acetylcholinesterase inhibitor. Of more significant concern, if left in the environment, some of

the products observed from the degradation of malathion can function as more potent toxins than the parent compound. These compounds may threaten human life if they are present in high quantities during operations in contaminated or industrial areas. Several experimental studies have been performed to elucidate the possible degradation products of malathion under various conditions to probe both the application of potential remediation methods and the environmental fate of the degradation products. However, only limited computational studies have been reported to delineate the mechanism by which malathion degrades under environmental conditions and how these degradation mechanisms are intertwined with one another. Herein, M06-2X DFT computations were employed to develop comprehensive degradation pathways from the parent malathion compound to a multitude of experimentally observed degradation products. These data corroborate experimental observations that multiple degradation pathways (ester hydrolysis and elimination) are in competition with each other, and the end-products can therefore be influenced by environmental factors such as temperature. Furthermore, the products resulting from any of the initial degradation pathways (ester hydrolysis, elimination, or P-S hydrolysis) can continue to degrade under the same conditions into compounds that are also reported to be toxic.

KEYWORDS: Malathion, cholinesterase inhibitor, DFT, degradation kinetics, environmental fate

*Corresponding author; email: Manoj.K.Shukla@usace.army.mil

## INTRODUCTION

Organophosphorus compounds (OPCs) are commonly found in herbicides, pesticides, and chemical warfare agents for much the same reason: they act as potent acetylcholinesterase inhibitors. From an environmental perspective, the accumulation of OPCs in the environment can negatively affect human health.[1] One such OPC, malathion, is used worldwide for pest control on a variety of crops.[2] Because of its widespread utilization and potential for toxicity as an OPC, extensive experimental studies have been conducted on the degradation of malathion under various conditions, the pesticide's effects on microbes and animals,[3-5] and the development and application of chemical or biological remediation techniques.[4, 6-21] However, there are limited

experimental studies that determine the intermediates and end-products of these degradation mechanisms, particularly under environmental conditions.[22]

Several computational studies have also been conducted to understand the experimentally observed degradation pathways better .[23-25] In 2008, Leszczynski and coworkers investigated the gas-phase mechanisms of alkaline hydrolysis for several phosphotriesterase substrates (DFP, paraoxon, parathion, and acephate) with DFT and post-HF *ab initio* techniques.[23] Reaction mechanisms tend to follow similar trends for structurally similar compounds, but malathion was not examined in this study. In 2014, Leszczynski and coworkers published a follow-up study on how the orientation of the incoming hydroxide ion can impact which P-chalcogen bond is cleaved and the underlying reaction mechanism (single-step vs. multi-step interchange). [24] While this study adds several OPCs, including malathion, it is still narrowly focused on the first step of the degradation pathway over the previous study. More recently, Chen et al.[14] have examined the hydrolysis of acephate by water, wherein the hydrolysis mechanism is determined for multiple points of the same molecule. This study does incorporate the possibility of competing reaction pathways; however, they are for a different, albeit related, compound, and they only consider the possibilities for the initial degradation step. Unfortunately, these investigations have tended to

focus on single aspects of the degradation pathway, typically the cleavage of the bonds about the P center, whereas under environmental conditions, multiple pathways may be in competition with each other. Moreover, the initial degradation products may continue to react further under the same conditions and should be considered for the detailed evaluation of degradation reaction mechanisms.

While these prior studies are useful for discussing the initial degradation steps of various OPCs, different computational methodologies have been employed in each of these investigations, thus precluding direct comparisons of the mechanistic pathways for the ones that do discuss malathion. However, under environmental conditions, the pathways in these studies can be intertwined, both with each other as well as with those leading to additional breakdown products, i.e., the hydrolysis of the ester groups of malathion before vs after hydrolysis at the phosphate center. To reliably determine how these previously established pathways and possible alternatives interconnect, they all require treatment with the same computational methodology. Herein, we aim to determine plausible mechanistic pathways to a variety of experimentally observed degradation products under alkaline conditions using Density Functional Theory. Additionally, because these pathways will be determined at the same level of theory, they can all

be directly compared to one another *and* to experimental data. This work and future efforts will be aimed at developing a more comprehensive understanding of how the possible degradation mechanisms and kinetics relate to each other under a variety of environmental conditions.

## COMPUTATIONAL DETAILS

All computations were performed using the C.01 Revision of the Gaussian 16 suite of programs.[26] All geometries were optimized with the M06-2X density functional,[27] the 6-31G(d,p) basis set (employing cartesian d functions),[28-30] and the IEFPCM implicit solvation model[31-51] using parameters consistent with water as the solvent. Additional, explicit water molecules were also used (except where noted) to stabilize the hydroxide ion and facilitate the optimization of intended species and transition states. For computational simplicity, all ethyl groups were truncated to methyl groups (See Figure S1 in supporting information). Optimized geometries were confirmed to be minima or transition states by a subsequent analytical frequency computation yielding 0 (minimum) or 1 (transition state) imaginary modes at the same level of theory. Transition states were also validated by connecting to respective reactants and products through the displacement of the TS geometry along the vector of the imaginary mode.

The resulting geometries of reactants and products obtained through this procedure were again fully optimized to ensure their correctness. More reliable energies were obtained using single-point energy computations with the more robust aug-cc-pVTZ[52, 53] basis set. Free energies at these single-point energy computations were obtained by applying the thermodynamic corrections from the M06-2X/6-31G(d,p) level of theory. The mechanistic discussion will use the relative energies from M06-2X/aug-cc-pVTZ//M06-2X/6-31G(d,p) level of theory. M06-2X is considered to provide reasonable thermodynamic data, is consistent with prior literature in using a triple-ζ basis set and is a fraction of the expense of analogous post-HF MP2 computations. For completeness of data relative to prior literature, post-HF *ab initio* MP2 computations[54-58] (MP2/aug-cc-pVTZ//M06-2x/6-31G(d,p)) were also performed and the analogous data are available in the Supporting Information (SI) section. Overall, the trends in the data from MP2 computations are qualitatively consistent with the M06-2X results, although the specific values are quite different. MP2 overestimating barrier heights is a known issue in the literature[59, 60] and thus the data from MP2 should only be considered with caution and with respect to prior literature on this subject. For transition states in which proton abstraction was the primary imaginary vibrational mode, tunneling corrections were computed using the small curvature

tunneling model (SCT) within the Polyrate 17-C and Gaussrate 17-B suites of programs.[61, 62] These corrections were found to be minor and are documented further in the SI. For operational simplicity, the discussion here will employ only the energies from transition state theory without tunneling corrections applied. All structural images were rendered in Chemcraft.[63]

## RESULTS AND DISCUSSION

### Degradation Mechanisms

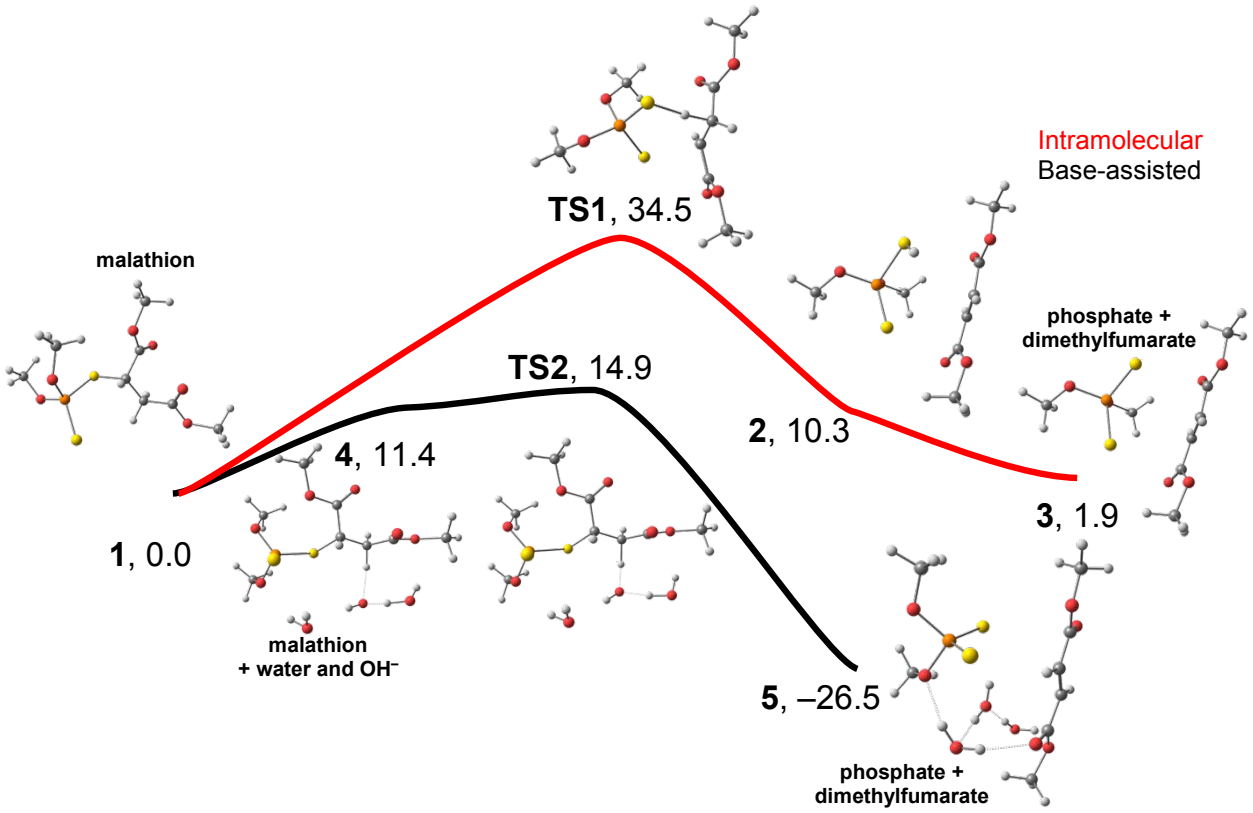

Figure 1. Intramolecular (**1** → **3**) vs base-assisted elimination (**4** → **5**) reactions of malathion at the M06-2X/aug-cc-pVTZ//M06-2X/6-31G(d,p) level of theory in bulk water. Bolded numbers denote the compound numbers and normal numbers are relative free energies in kcal $mol^{-1}$. Atom colors are as follows C: gray, P: orange, H: white, S: yellow, O: red.

A commonly debated degradation mechanism for malathion under alkaline conditions is elimination to diethyl fumarate vs hydrolysis to a malathion monoacid. First examining the elimination pathway, as shown in Figure 1, malathion can undergo intramolecular elimination to a P-*O*,*O*,*S*,*S* phosphate and dimethyl fumarate, **2**. However, the transition state (**TS1**) for intramolecular elimination is prohibitively high in energy (34.5 kcal $mol^{-1}$). Base-assisted elimination is significantly more viable. In aqueous solution, malathion would have several hydrogen-bonding interactions with the solvent. Unfortunately, these interactions are difficult to model computationally; therefore, only two explicit water molecules were incorporated to stabilize the presence of the hydroxide ion. The initial association of the water and hydroxide molecules, **4**, from bulk solution (obtained from separate computations on isolated water and hydroxide molecules with implicit solvation) is endergonic by about 11.4 kcal/mol. With a proximal hydroxide ion, the barrier to remove a proton from the bis-ester chain and the formation

of dimethyl fumarate and P-*O*,*O*,*S*,*S* phosphate (products **5**) is less than 4 kcal $mol^{-1}$. Additionally, the formation of products **5** from hydroxide serves as a significant thermodynamic driving force for this pathway. Experimentally, an appreciable quantity of the elimination products diethyl fumarate and ethyl hydrogen fumarate are observed in addition to the ester hydrolysis products after a single half-life of malathion under alkaline conditions.[22] A reasonably accessible transition state, as shown in Figure 1, is in line with experimental observations. Additionally, the presence of ethyl hydrogen fumarate experimentally indicates that the initial elimination product, diethyl fumarate, continues to degrade under alkaline conditions. These data may be important to consider in the overall toxicity picture as diethyl fumarate is a more potent toxin to aquatic life than malathion.[64]

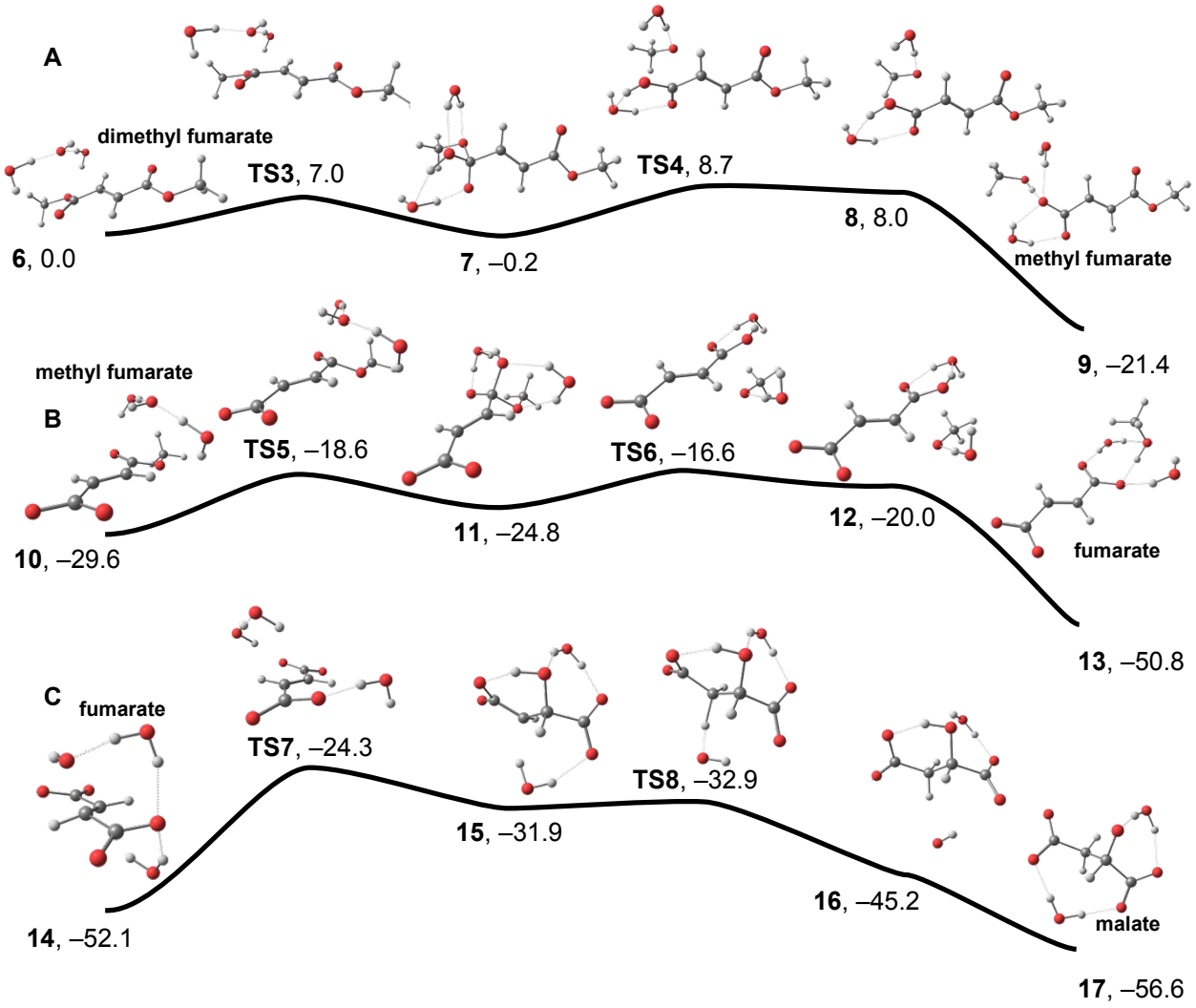


Figure 2. Sequential hydrolysis of A) dimethyl fumarate to methyl fumarate (**6** → **9**) B) methyl fumarate to fumarate (**10** → **13**) and C) fumarate to malate (**14** → **17**) at the M06-2X/aug-cc-pVTZ//M06-2X/6-31G(d,p) level of theory in bulk water. Bolded numbers denote the compound numbers and normal numbers are relative free energies in kcal $mol^{-1}$. Atom colors are as follows C: gray, P: orange, H: white, S: yellow, O: red.

Because the hydrolysis products of the fumarate ester have been observed experimentally,[22, 65] and diethyl fumarate has been shown to be toxic to aquatic life,[64] its complete hydrolysis reaction pathway (as dimethyl fumarate for computational simplicity) was also computed. A proximal hydroxide ion attacks one of the carbonyl carbons of dimethyl fumarate, **6**, creating the tetrahedral intermediate **7**. Subsequent loss of methoxide generates the monoacid **8**, which then deprotonates to form the corresponding carboxylate **9** and methanol (MeOH). The total process of liberating MeOH (**6** to **9**) is exergonic by ~21 kcal $mol^{-1}$. The monoacid carboxylate **10** can undergo further hydrolysis that results in the fumarate ion **13** and an additional MeOH. During this process (**10** to **13**), the liberation of MeOH is again exergonic by ~21 kcal $mol^{-1}$. This significant drop in energy serves as a thermodynamic driving force for these reactions, although the second hydrolysis is predicted to proceed slower than the first with $\Delta\Delta G^{\ddagger}$ of ~8 kcal $mol^{-1}$ vs ~13 kcal $mol^{-1}$ for dimethyl and methyl fumarate, respectively. Given the relatively low TS energies, under even mildly alkaline conditions, dimethyl fumarate would be expected to at least partially degrade to methyl fumarate and fumarate. The final step is the base catalyzed hydration of the olefin in a two-step process. The olefin **14** undergoes nucleophilic attack by a hydroxide ion resulting in a carbanion intermediate **15**. This intermediate then deprotonates a neighboring

water molecule to form malate and regenerate hydroxide ion, **16**. The resulting hydroxy group can also be deprotonated to create the trianion **17**. This final hydrolysis of fumarate to malate is expected to proceed significantly slower than the ester hydrolysis ($\Delta\Delta G^{\ddagger}$ of ~20 kcal mol$^{-1}$). While this transition state is possible, the malate product was not observed to any appreciable extent experimentally.[22] Interestingly, the exchange of methanol for a new hydroxide from bulk solution (i.e., **9** → **10** and **13** → **14**) is slightly exergonic (–8.2 and –1.3 kcal mol$^{-1}$, respectively). Recall that in the elimination mechanism in Figure 1, the association of a hydroxide ion from bulk solution was endergonic. However, in Figure 2, the hydroxide ion and water molecules have a different hydrogen bonding configuration, which may explain these differences. In either case, the relative energies for the steps involving associating a hydroxide ion from solution should be taken with a degree of caution as these trends are subject to some methodological variation (see Tables S1 and S2 in the SI).

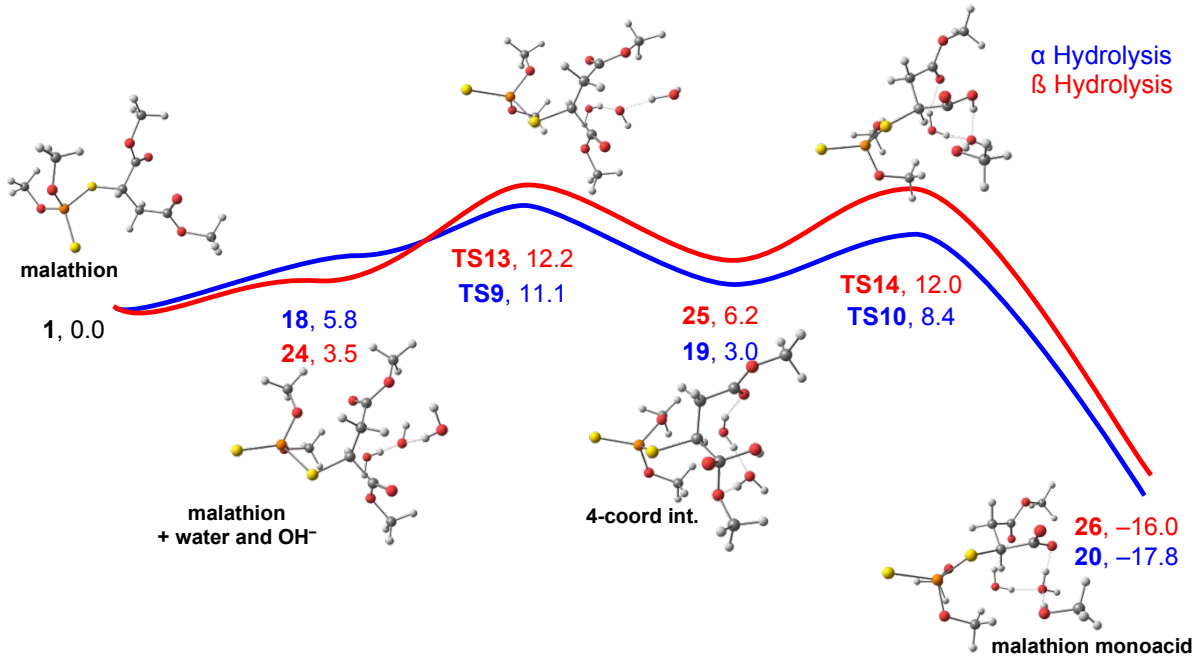


Figure 3. α- vs ß-ester hydrolysis (**18** → **20** or **24** → **26**) at the M06-2X/aug-cc-pVTZ//M06-2X/6-31G(d,p) level of theory in bulk water. Bolded numbers denote the compound numbers and normal numbers are relative free energies in kcal $mol^{-1}$. Atom colors are as follows C: gray, P: orange, H: white, S: yellow, O: red. Only the structures for hydrolysis of the α ester are shown; ß is structurally similar.

As mentioned previously, a common alternative to the elimination pathway is the hydrolysis of the ester chains to malathion α- and ß-monoacids. As shown in Figure 3, bringing the hydroxide ion from the bulk solution proximal to either the α or ß carbonyls (**18** and **24**) is essentially isoenergetic. The transition state for nucleophilic attack of the hydroxide ion to form the

tetrahedral intermediate is only slightly lower for the α position, (11.1 kcal mol$^{-1}$, **TS9**) as opposed to the ß position (12.2 kcal mol$^{-1}$, **TS13**). The relative energies of the resulting tetrahedral intermediates (3.0 vs. 6.2 kcal mol$^{-1}$, **19** and **25**) demonstrate that attack at the α position is kinetically favorable and forms the thermodynamic product. The second step of the hydrolysis occurs primarily as a dissociation of the methoxide ion; simultaneously, a proton is transferred from a neighboring water to the methoxide, that water molecule deprotonates the COOH. The net result is a loss of MeOH from the parent compound and formation of the malathion monoacid anion (**20** and **26**). Throughout this process, the α and ß positions remain energetically similar, indicating that both could be observed experimentally, with the α-monoacid being in a slight excess. The trends in these data are indeed observed experimentally.[22] Concerning the interplay between the elimination and hydrolysis pathways, the initial placement of the proximal hydroxide ions (species **4**, **18**, and **24**) are quite different energetically at 11.4 vs 5.8 vs 3.5 kcal mol$^{-1}$, respectively (Figures 1 and 3). Based on these minima, there will likely be a significantly higher population poised for ester hydrolysis rather than the elimination pathway. In a similar vein, the corresponding free energy of activation for each of the transition states are quite close (14.9, 12.2 and 11.1 kcal mol$^{-1}$, respectively; Figures 1 and 3) and are each accessible

at room temperature. However, the transition state for the elimination reaction is the highest among them at 14.9 kcal $mol^{-1}$. Given these data, the hydrolyses are likely to proceed to a greater extent than the elimination, although products from both will likely be observed. These conclusions are consistent with experimental data where at pH 8 and 27 °C, the ester hydrolysis and elimination reactions were found to be in competition. Additionally, experimental data suggest that elimination is favored at higher temperatures while ester hydrolysis is favored at lower temperatures.[22] The data in Figure 3 corroborate the experimental data. Ester hydrolysis is the kinetically favored pathway and will be more accessible at lower temperatures, whereas the elimination pathway produces the thermodynamic product, but has a higher free energy of activation.

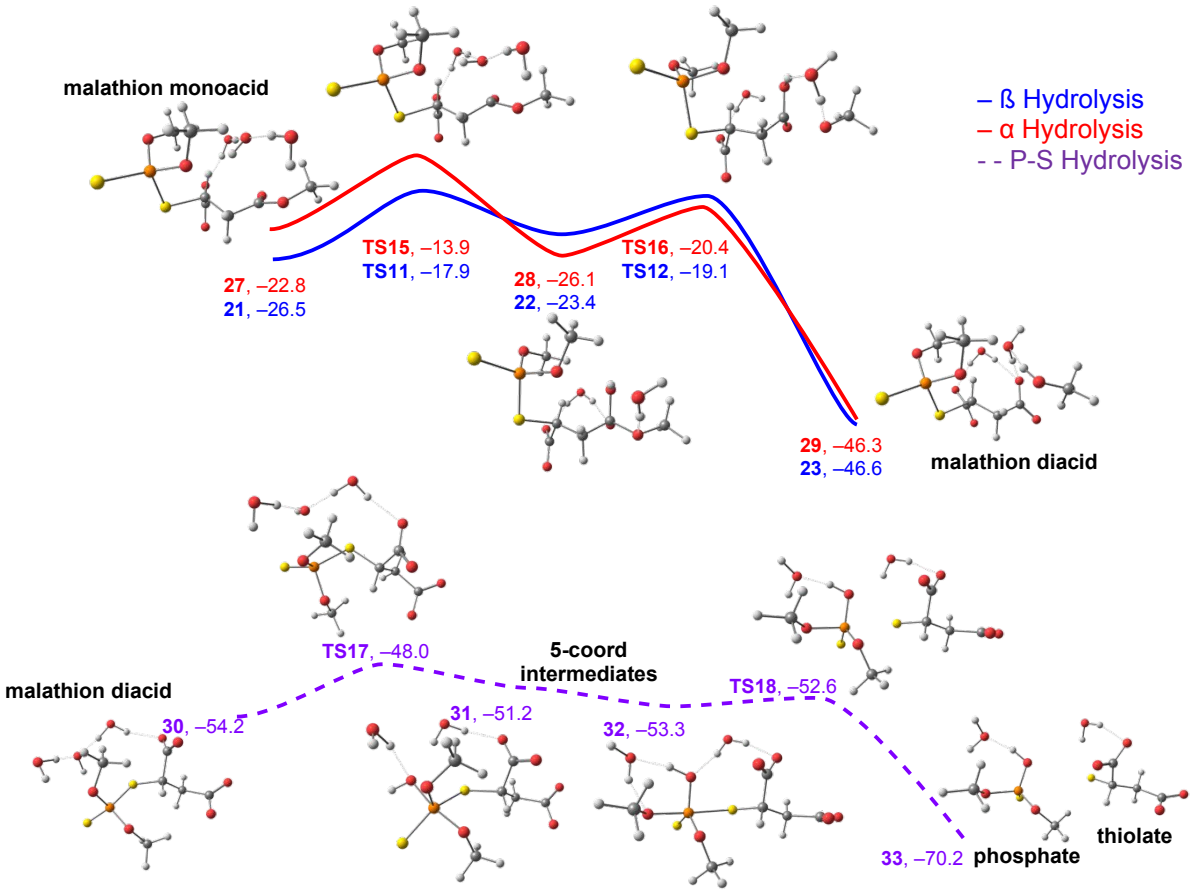


Figure 4. Hydrolysis of monoacid ester (**27** → **29** or **21** → **23**) and subsequent hydrolysis of P-S bond (**30** → **33**) at the M06-2X/aug-cc-pVTZ//M06-2X/6-31G(d,p) level of theory in bulk water. Bolded numbers denote the compound numbers and normal numbers are relative free energies in kcal mol$^{-1}$. Atom colors are as follows C: gray, P: orange, H: white, S: yellow, O: red. Only structures for hydrolysis of ß ester are shown (a continuation of the reaction sequence from Figure 3 where the α ester has already been hydrolyzed); α is structurally similar.

Following the formation of the α- and ß-monoacids, the ester groups can be further hydrolyzed to the diacid (**23** and **29**), as shown in Figure 4. As before, both pathways are energetically similar and should proceed at similar rates. Although, hydrolysis of either the α- or ß-monoacids (**21** or **27**) will likely be slower than the ester hydrolysis of malathion ($\Delta\Delta G^{\ddagger}$ of ~10 kcal $mol^{-1}$ for the monoacids vs $\Delta\Delta G^{\ddagger}$ of ~7 kcal $mol^{-1}$ for the diacids). This assignment is qualitatively consistent with experimental data, although the experimental data have the monoacid hydrolyses proceeding significantly slower than malathion.[22] After generating the malathion diacid, the P-S bond can also be hydrolyzed. The P center undergoes nucleophilic attack by the hydroxide ion resulting in a trigonal bipyramidal intermediate **31** wherein both S atoms and one methoxy group occupy the equatorial positions. This intermediate then reorganizes to **32,** which places the P-S-C moiety in the axial position. Dissociation of the P-S bond results in the formation of a phosphate and a thiolate, **33**. Prior literature has evaluated the viability of an associative interchange transition state whereby the thiolate is exchanged for hydroxide in a single reaction step.[24] This interchange transition state was regularly found to be isoenergetic or slightly endergonic relative to the two-step exchange process; thus only the two-step process was investigated here. Combined data for Figure 3 and Figure 4 from each methodology are tabulated in Table S3, and

the P-S hydrolysis data from Figure 4 are available in Table S4. Overall, the subsequent hydrolyses of the monoacid to the diacid and the diacid to separate phosphate and thiolate compounds are all exergonic. Moreover, these reactions are easily accessible with relatively low free energies of activation for each of the transition states. These data further demonstrate that the initial hydrolysis is not the end of the degradation pathway for these compounds; in fact they can easily continue to degrade into additional organophosphate compounds, one of which (**33**) is a known toxin to aquatic life.[64]

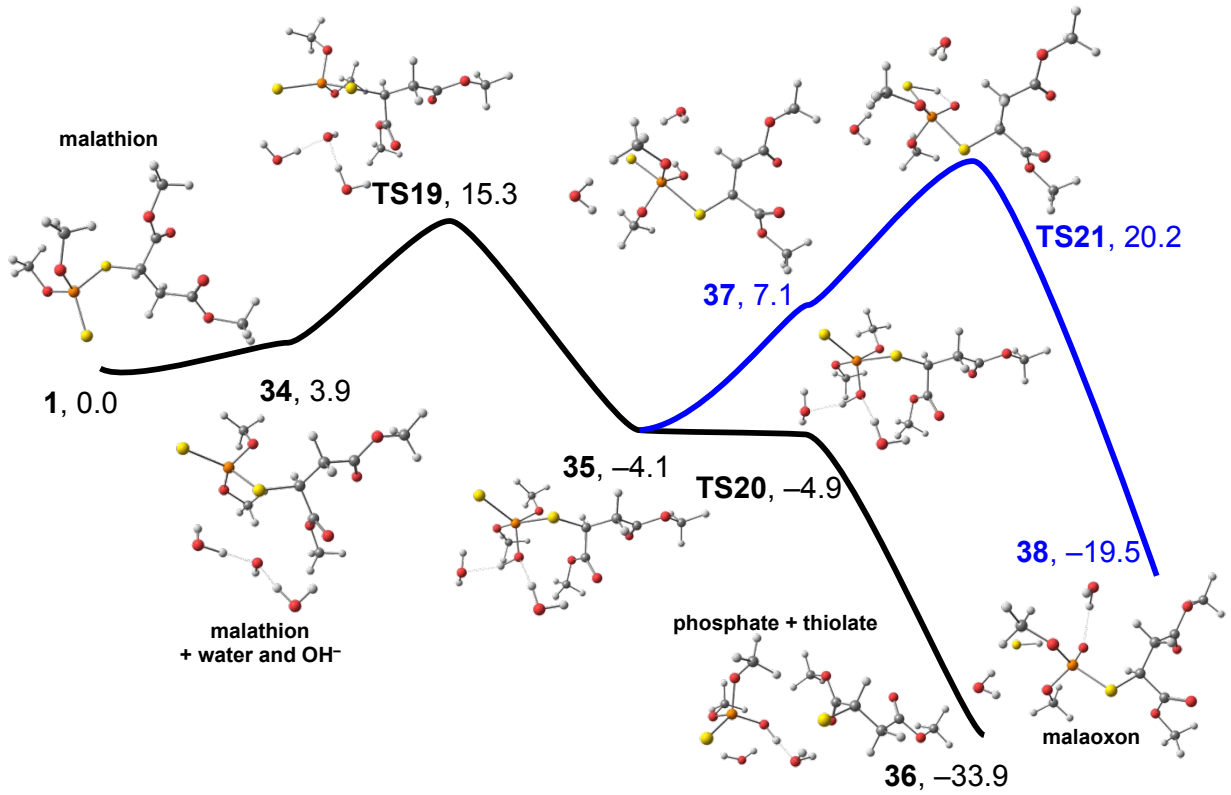

Figure 5. Hydrolysis of the P-S bonds of malathion at the M06-2X/aug-cc-pVTZ//M06-2X/6-31G(d,p) level of theory in bulk water. Bolded numbers denote the compound numbers and normal numbers are relative free energies in kcal $mol^{-1}$. Atom colors are as follows C: gray, P: orange, H: white, S: yellow, O: red.

The P-S bonds of malathion could be hydrolyzed prior to the ester groups. In this scenario, as shown in Figure 5, the P center of **34** undergoes nucleophilic attack by the hydroxide ion resulting in a trigonal bipyramidal intermediate **35** wherein the hydroxide, P=S moiety, and one methoxy group occupy the equatorial positions. Breaking the P-S bond from the P-S-C moiety in this scenario is a barrierless transition resulting in a phosphate (*O,O*-dimethyl phosphorothioic acid) and a thiolate species, **36**. This breakdown pathway was not observed experimentally under alkaline conditions,[22] and the absence of these products is corroborated by the computational data given that **TS19** (Figure 5) is higher in energy than **TS2** (Figure 1), **TS9**, or **TS13** (Figure 3).

From the same trigonal bipyramidal intermediate **35**, an alternative, higher energy pathway exists wherein the P=S moiety migrates from an equatorial position to an axial position, **37** (Figure 5). From this geometry, the OH proton can be transferred to the P=S sulfur atom, resulting in immediate loss of a bisulfide ion and formation of malaoxon, **38**. Previous studies

have evaluated the conversion of structurally similar parathion to paraoxon via a similar attack of hydroxide ion.[23, 24] To our knowledge, a plausible conversion to malaoxon proceeding from a hydroxide ion has not been reported for malathion. These data show that such a transformation is possible, although it is notably higher in energy than competing hydrolytic degradation pathways. Therefore, while technically possible, malathion is not anticipated to convert to malaoxon to any appreciable extent under environmental conditions and experimental data corroborate this assignment.[22]

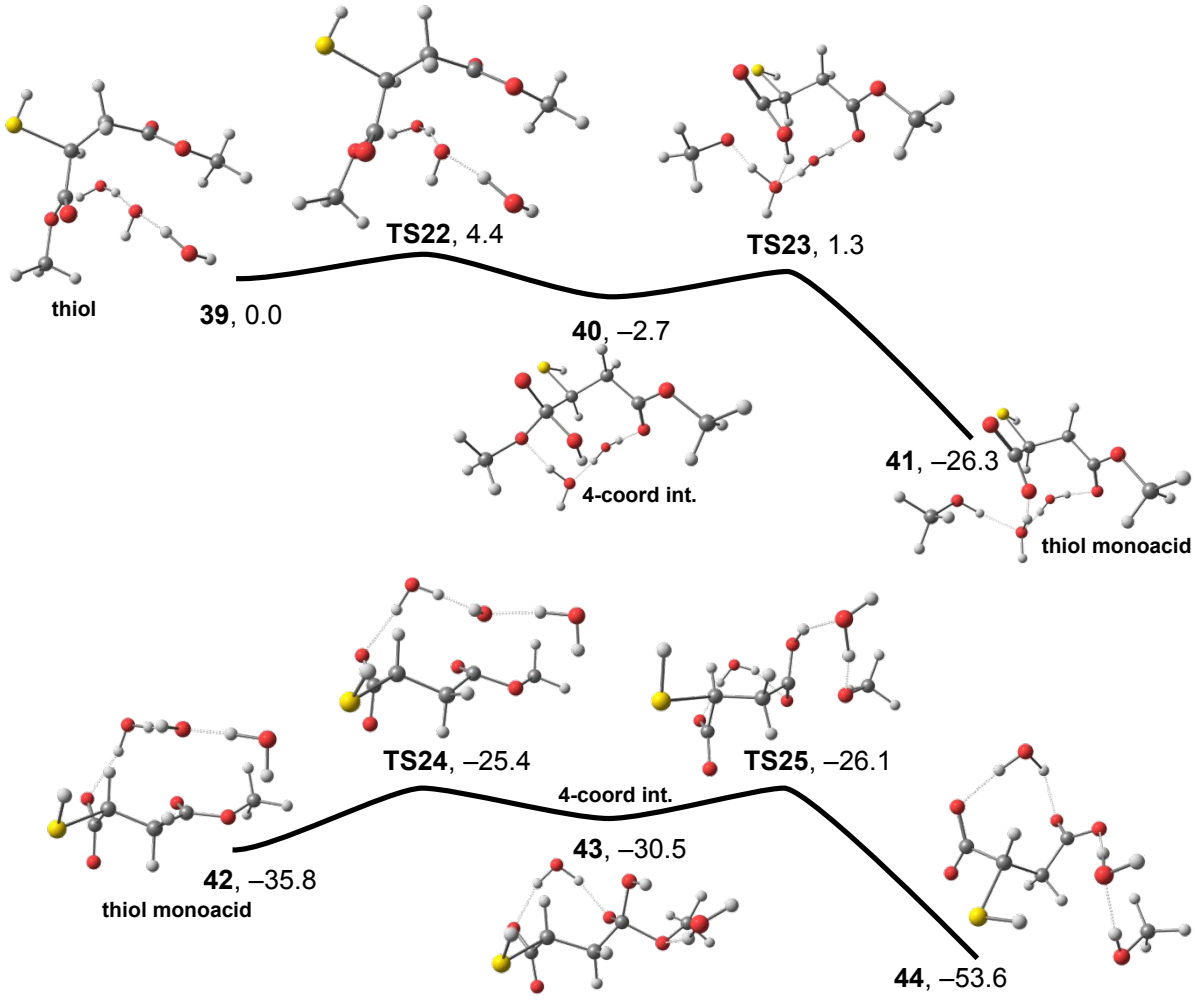


Figure 6. Sequential hydrolysis of the ester groups (α then ß) from the bis-ester thiol at the M06-2X/aug-cc-pVTZ//M06-2X/6-31G(d,p) level of theory in bulk water. Bolded numbers denote the compound numbers and normal numbers are relative free energies in kcal $mol^{-1}$. Atom colors are as follows C: gray, P: orange, H: white, S: yellow, O: red.

Because the thiol is a weak acid (see SI), following hydrolysis of the P-S bond to a phosphate and thiolate, **36**, the thiolate will pick up a proton from solution to form the corresponding thiol. The thiol ester groups can then be hydrolyzed as shown in Figure 6. The association of the hydroxide to the α carbonyl, **39**, has only small free energy of activation to form the tetrahedral intermediate, **40**. Subsequent dissociation of methoxide ion and proton transfer results in the loss of MeOH and formation of the carboxylate ion, **41**. Repeating the hydrolysis for the ß carbonyl group (bottom pathway in Figure 6) forms another MeOH and the dicarboxylate thiol, **43**. Given the very low free energies of activation, thiol **39** will likely not be observed under alkaline conditions. However, hydrolysis of the monoacid thiol will be significantly slower than the thiol ($\Delta\Delta G^{\ddagger}$ of ~10 kcal $mol^{-1}$ vs $\Delta\Delta G^{\ddagger}$ of ~4 kcal $mol^{-1}$), although it is comparable to the rate of ester hydrolysis of malathion indicating that any amount of thiol generated from the previous step in Figure 5 will likely only exist as the thiol dicarboxylate **44**. If this pathway were to be observed experimentally, it would most likely be detected via the *O,O*-dimethyl phosphorothioic acid in **36** or the thiol dicarboxylate **44**. Combined data (Figure 6)Figure 5 from each methodology are tabulated in Table S6.

The computed data presented herein demonstrate that the initial hydrolysis of the parent malathion is not the end of the degradation pathway under alkaline conditions. The free energies of activation for several transition states are easily accessible at room temperature and the end products are quite exergonic. Several of the resulting products are not as toxic as the parent malathion; however, the degradation products which are phosphate-containing compounds or fumarate-based are notably toxic to aquatic life.[64] Thus, any degradation pathways that result in such compounds, not only direct generation from the parent compound, should be considered for both malathion and structurally similar compounds.

## Degradation Kinetics

Preliminary kinetics of the initial malathion degradation discussed above have been developed from the activation energies from each pathway (Figures 1-6). The uni- and bimolecular rate constants were calculated using a formalism based on the Eyring equation as show in the following equations:

$$k_{uni} = \frac{kT}{h} e^{\Delta G_T^{\ddagger}/RT} \quad (s^{-1}) \qquad (1)$$

$$k_{bi} = \frac{kT}{h} e^{\Delta G_T^{\ddagger}/RT} \left(\frac{1}{c}\right) \quad (L \cdot mol^{-1} \cdot s^{-1}) \qquad (2)$$

In equations 1 and 2, $k$ is Boltzmann's constant, $T$ is temperature, $h$ is Planck's constant, $R$ is the gas constant, and $\Delta G_T^{\ddagger}$ is the activation energy; $c$ (in equation 2) is a unit transformation coefficient equivalent to 1 mol/L. A system of equations was generated for each species in the reaction pathway using the approach shown below:

$$\sum_i \frac{dn_i}{dt} = \sum_{\substack{i \\ j \neq i}} k_{ij} n_j - n_i \sum_{\substack{l \\ l \neq i}} k_{il} \quad (3)$$

$$\sum_i \frac{dn_i}{dt} = \sum_{\substack{j \\ j,m \neq i}} k_{ij} n_j n_m - n_i \sum_{\substack{l \\ l,o \neq i}} k_{il} n_o \quad (4)$$

where $n_i$ correspond to chemical species and the $k_i$ are rate constants.

Figure 7 illustrates the predicted kinetics for the loss of malathion and the formation of various degradation products over time. Due to the low activation barrier (see black curve in Figure 1), malathion almost instantaneously degrades into dimethyl fumarate and a dimethyl phosphorodithioic acid (DPTA) upon exposure to $OH^-$ ion (Figure 1, complex **5**). In Figure 7, DPTA is the brown horizontal curve with a stable concentration slightly under 0.001 mol/L (0.001 mol/L was the initial malathion concentration in the kinetics calculations). Similar to the rapid disappearance of malathion, the dimethyl fumarate instantly converts to methyl fumarate

and methanol upon exposure to $OH^-$ ion. Methyl fumarate further hydrolyzes to give fumarate and more methanol. Methyl fumarate (purple curve) and fumarate (yellow curve) are essentially inverses of one another as the former decays and the latter forms. Additionally, the methanol curve (red) levels off at slightly under 0.002 mol/L. The final curve in Figure 7 is for a dimethyl phosphorothionic acid, which arises from the hydrolysis of the P-S bond in malathion (see Figure 5, complex **36**). The small amount of the thionic acid formed accounts for the slightly less than 0.001 mol/L of the dithioic acid formed in Figure 1.

The formation of degradation products is limited by the amount of $OH^-$ present. In the pathways presented here, approximately 0.001 mol/L of $OH^-$ immediately reacts with malathion (until consumed). The degradation of dimethyl fumarate to fumarate consumes the bulk of the remaining $OH^-$. Our results are in qualitative agreement with Wolfe et al.,[15] in which a primary degradation product was the ethyl form of DPTA although the carboxyl ester hydrolysis products were also observed indicating that competing reaction mechanisms are present under alkaline conditions at 27 °C. Based on our computed data on the initial degradation step (Figure 3), the elimination reaction and ester hydrolyses will likely be in competition with each other with the elimination reaction leading to the thermodynamic product and the ester hydrolyses leading to

kinetic products. The presence of both reaction products experimentally, combined with the temperature dependence on product preference are qualitatively consistent with the computed data. Although, some aspects of the kinetics results are difficult to compare. The data in Figure 7 indicate that that malathion degrades near instantaneously, whereas the experimental half-life of malathion is recorded at approximately 36 hours.[22] We believe that the excess of $OH^-$ ion (3:1 initial $OH^-$ to malathion) results in our system of reactions predicting much more rapid degradation compared to experiment.

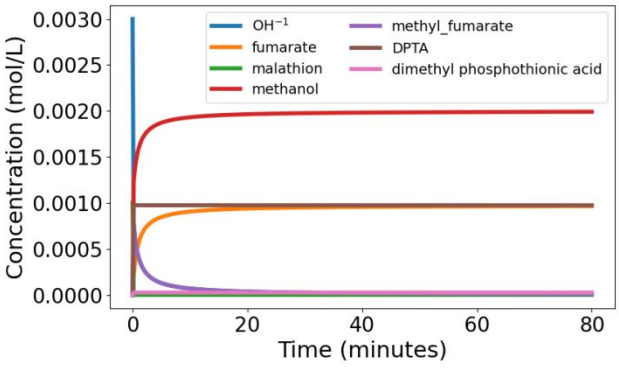


Figure 7. Kinetics for select species from the malathion degradation pathway. Initial conditions for [$OH^-$] and [malathion] were 0.003 M and 0.001 M, respectively.

## CONCLUSIONS

This work presents a comprehensive, atomistic perspective of the multiple degradation pathways of malathion under alkaline conditions. Each of these pathways has now been studied at the same level of theory for direct comparison to one another allowing for greater insight into the impact of the reaction environment on the directions of the potential mechanism. Based on our data, we found that, in correlation with experimental observations, elimination and ester hydrolysis are in competition with each; ester hydrolysis favored at lower temperatures and elimination favored at higher temperatures. Hydrolysis of the P-S bond is accessible, although higher in energy than ester hydrolysis or elimination and thus less likely to significantly contribute. Still all of these pathways are kinetically accessible and will be in competition with each other. The conversion to malaoxon (via attack by hydroxide) is also kinetically accessible at room temperature, although it is notably higher than the other pathways and thus will likely have little contribution to the overall picture. Following an initial breakdown of malathion by any of these mechanisms, subsequent hydrolyses to additional products (i.e. malate, a biscarboxythiolate, P-*O*,*O*,*O*,*S* phosphate **33**, etc.) are exergonic with low-lying transition states. It is expected that any initial breakdown products from malathion will further degrade into these smaller components if left in the environment unremedied. Given that some of the degradation

products have also been found to be toxic to aquatic life (e.g. diethyl fumarate and DMPTA) their degradation mechanisms should be incorporated into toxicity and remediation considerations. Hydroxyl radical is also present under alkaline conditions, and as such, efforts are currently underway to examine the impact of hydroxyl radical on the pathways computed here. Further establishing the relationship between hydroxide and hydroxyl radical within the web of possible degradation pathways will be useful in understanding how malathion is degraded under both environmental and biological conditions.

## ASSOCIATED CONTENT

**Supporting Information**.

The following files are available free of charge.

Supplementary Schemes and tabulated energies (PDF)

Molecular coordinates of computed structures (XYZ)

## AUTHOR INFORMATION

**Corresponding Author**

*Manoj.K.Sukla@usace.army.mil

## Author Contributions

The manuscript was written through contributions of all authors. All authors have given approval to the final version of the manuscript.

## Funding Sources

N/A

## ACKNOWLEDGMENT

The use of trade, product, or firm names in this report is for descriptive purposes only and does not imply endorsement by the U.S. Government. The tests described and the resulting data presented herein, unless otherwise noted, were obtained from research funded under the Installations and Operational Environments, Office of the Technical Director of the United States Army Corps of Engineers, and the Environmental Security Technology Certification Program of the Department of Defense by the USAERDC. Permission was granted by the Chief of Engineers to publish this information. The findings of this report are not to be considered as an official Department of the Army position unless so designated by other authorized documents. This work

was supported by a grant of computer time from the DoD High Performance Computing Modernization Program at ERDC, Vicksburg, MS. This document has been approved for public release (Distribution Statement A) by the Engineer Research and Development Center.

## REFERENCES

1. F. M. Raushel, Catalytic detoxification, *Nature*, 2011, **469**, 310-311.
2. G. Sankaran, L. Chen, Z. Chen, Y. Liu, T. Lopez, J. Ross, S. Phagura, D. A. Eastmond and R. I. Krieger, The Importance of Hand Exposures to Absorbed Dosage of Hand Harvesters, *J. Toxicol. Environ. Health, Part A*, 2015, **78**, 1369-1383.
3. W. E. Cotham and T. F. Bidleman, Degradation of malathion, endosulfan, and fenvalerate in seawater and seawater/sediment microcosms, *J. Agric. Food Chem.*, 1989, **37**, 824-828.
4. A. K. Janeczko, E. B. Walters, S. J. Schuldt, M. L. Magnuson, S. A. Willison, L. M. Brown, O. N. Ruiz, D. L. Felker and L. Racz, Fate of malathion and a phosphonic acid in activated sludge with varying solids retention times, *Water Res.*, 2014, **57**, 127-139.
5. K. Newhart, *Environmental Fate of Malathion*, C. E. P. Agency, 2006.
6. B. T. Bowman, R. S. Adams and S. W. Fenton, Effect of water upon malathion adsorption onto five montmorillonite systems, *J. Agric. Food Chem.*, 1970, **18**, 723-727.
7. L. Lin, M. Xie, Y. Liang, Y. He, G. Y. Sing Chan and T. Luan, Degradation of cypermethrin, malathion and dichlorovos in water and on tea leaves with O3/UV/TiO2 treatment, *Food Control*, 2012, **28**, 374-379.
8. X.-J. Luo, J. Zhao, C.-X. Li, Y.-P. Bai, M. T. Reetz, H.-L. Yu and J.-H. Xu, Combinatorial evolution of phosphotriesterase toward a robust malathion degrader by hierarchical iteration mutagenesis, *Biotechnol. Bioeng.*, 2016, **113**, 2350-2357.
9. S. Kanagasubbulakshmi, R. Kathiresan and K. Kadirvelu, Structure and physiochemical properties based interaction patterns of organophosphorous pesticides with quantum dots: Experimental and theoretical studies, *Colloids and Surfaces A: Physicochemical and Engineering Aspects*, 2018, **549**, 155-163.

10. M. Mehdipour, M. Ansari, M. Pournamdari, L. Zeidabadinejad and M. Kazemipour, Selective extraction of organophosphorous pesticides in plasma by magnetic molecularly imprinted polymers with the aid of computational design, *Analytical Methods*, 2018, **10**, 4136-4142.

11. Y. Liu, S. Liu, Y. Zhang, D. Qin, Z. Zheng, G. Zhu, Y. Lv, Z. Liu, Z. Dong, X. Liao and X. Li, The degradation behaviour, residue distribution, and dietary risk assessment of malathion on vegetables and fruits in China by GC-FPD, *Food Control*, 2020, **107**, 106754.

12. H. Yu, X. Wang, H. Sun and M. Huo, Photocatalytic degradation of malathion in aqueous solution using an Au–Pd–TiO2 nanotube film, *J. Hazard. Mater.*, 2010, **184**, 753-758.

13. F. Matsumura and G. M. Boush, Malathion Degradation by Trichoderma viride and a Pseudomonas Species, *Science*, 1966, **153**, 1278-1280.

14. S. Xie, J. Liu, L. Li and C. Qiao, Biodegradation of malathion by Acinetobacter johnsonii MA19 and optimization of cometabolism substrates, *Journal of Environmental Sciences*, 2009, **21**, 76-82.

15. Y. Vasseghian, M. Moradi, M. Pirsaheb, A. Khataee, S. Rahimi, M. Y. Badi and A. Mousavi Khaneghah, Pesticide decontamination using UV/ferrous-activated persulfate with the aid neuro-fuzzy modeling: A case study of Malathion, *Food Research International*, 2020, **137**, 109557.

16. N. A. Ramos-Delgado, L. Hinojosa-Reyes, I. L. Guzman-Mar, M. A. Gracia-Pinilla and A. Hernández-Ramírez, Synthesis by sol–gel of WO3/TiO2 for solar photocatalytic degradation of malathion pesticide, *Catal. Today*, 2013, **209**, 35-40.

17. M. I. Swasy, B. R. Brummel, C. Narangoda, M. F. Attia, J. M. Hawk, F. Alexis and D. C. Whitehead, Degradation of pesticides using amine-functionalized cellulose nanocrystals, *RSC Advances*, 2020, **10**, 44312-44322.

18. A. N. Kadam, R. S. Dhabbe, M. R. Kokate, Y. B. Gaikwad and K. M. Garadkar, Preparation of N doped TiO2 via microwave-assisted method and its photocatalytic activity for degradation of Malathion, *Spectrochim. Acta Mol. Biomol. Spectrosc.*, 2014, **133**, 669-676.

19. S. Nasseri, M. Omidvar Borna, A. Esrafili, R. Rezaei Kalantary, B. Kakavandi, M. Sillanpää and A. Asadi, Photocatalytic degradation of malathion using Zn2+-doped TiO2

nanoparticles: statistical analysis and optimization of operating parameters, *Applied Physics A*, 2018, **124**, 175.

20. X. Chai, Y. Cui, W. Xu, L. Kong, Y. Zuo, L. Yuan and W. Chen, Degradation of malathion in the solution of acetyl peroxyborate activated by carbonate: Products, kinetics and mechanism, *J. Hazard. Mater.*, 2021, **407**, 124808.

21. S. M. Kanan, M. C. Kanan and H. H. Patterson, Photophysical Properties of Ag(I)-exchanged Zeolite A and the Photoassisted Degradation of Malathion, *J. Phys. Chem. B*, 2001, **105**, 7508-7516.

22. N. L. Wolfe, R. G. Zepp, J. A. Gordon, G. L. Baughman and D. M. Cline, Kinetics of chemical degradation of malathion in water, *Environ. Sci. Technol.*, 1977, **11**, 88-93.

23. E. Dyguda-Kazimierowicz, W. A. Sokalski and J. Leszczynski, Gas-Phase Mechanisms of Degradation of Hazardous Organophosphorus Compounds: Do They Follow a Common Pattern of Alkaline Hydrolysis Reaction As in Phosphotriesterase?, *J. Phys. Chem. B*, 2008, **112**, 9982-9991.

24. E. Dyguda-Kazimierowicz, S. Roszak and W. A. Sokalski, Alkaline Hydrolysis of Organophosphorus Pesticides: The Dependence of the Reaction Mechanism on the Incoming Group Conformation, *J. Phys. Chem. B*, 2014, **118**, 7277-7289.

25. R. Chen, L. Zhang, X. Luo and G. Liang, Hydrolysis of an organophosphorus pesticide: a theoretical investigation of the reaction mechanism for acephate, *Theor. Chem. Acc.*, 2018, **137**, 119.

26. M. J. T. Frisch, G. W.; Schlegel, H. B.; Scuseria, G. E.; Robb, M. A.; Cheeseman, J. R.; Scalmani, G.; Barone, V.; Petersson, G. A.; Nakatsuji, H.; Li, X.; Caricato, M.; Marenich, A. V.; Bloino, J.; Janesko, B. G.; Gomperts, R.; Mennucci, B.; Hratchian, H. P.; Ortiz, J. V.; Izmaylov, A. F.; Sonnenberg, J. L.; Williams-Young, D.; Ding, F.; Lipparini, F.; Egidi, F.; Goings, J.; Peng, B.; Petrone, A.; Henderson, T.; Ranasinghe, D.; Zakrzewski, V. G.; Gao, J.; Rega, N.; Zheng, G.; Liang, W.; Hada, M.; Ehara, M.; Toyota, K.; Fukuda, R.; Hasegawa, J.; Ishida, M.; Nakajima, T.; Honda, Y.; Kitao, O.; Nakai, H.; Vreven, T.; Throssell, K.; Montgomery, J. A., Jr.; Peralta, J. E.; Ogliaro, F.; Bearpark, M. J.; Heyd, J. J.; Brothers, E. N.; Kudin, K. N.; Staroverov, V. N.; Keith, T. A.; Kobayashi, R.; Normand, J.; Raghavachari, K.; Rendell, A. P.; Burant, J. C.; Iyengar, S. S.; Tomasi, J.; Cossi, M.; Millam, J. M.; Klene, M.; Adamo, C.; Cammi, R.; Ochterski,

J. W.; Martin, R. L.; Morokuma, K.; Farkas, O.; Foresman, J. B.; Fox, D. J., Gaussian 16 C.01, Gaussian, Inc., Wallingford, CT, USA, 2016

27. Y. Zhao and D. G. Truhlar, The M06 suite of density functionals for main group thermochemistry, thermochemical kinetics, noncovalent interactions, excited states, and transition elements: two new functionals and systematic testing of four M06-class functionals and 12 other functionals, *Theor. Chem. Acc.*, 2008, **120**, 215-241.

28. M. M. Francl, W. J. Pietro, W. J. Hehre, J. S. Binkley, M. S. Gordon, D. J. DeFrees and J. A. Pople, Self-consistent molecular orbital methods. XXIII. A polarization-type basis set for second-row elements, *J. Chem. Phys.*, 1982, **77**, 3654-3665.

29. M. S. Gordon, J. S. Binkley, J. A. Pople, W. J. Pietro and W. J. Hehre, Self-consistent molecular-orbital methods. 22. Small split-valence basis sets for second-row elements, *J. Am. Chem. Soc.*, 1982, **104**, 2797-2803.

30. P. C. Hariharan and J. A. Pople, The influence of polarization functions on molecular orbital hydrogenation energies, *Theor. Chim. Acta*, 1973, **28**, 213-222.

31. S. Miertuš, E. Scrocco and J. Tomasi, Electrostatic interaction of a solute with a continuum. A direct utilizaion of AB initio molecular potentials for the prevision of solvent effects, *Chem. Phys.*, 1981, **55**, 117-129.

32. S. Miertuš̃ and J. Tomasi, Approximate evaluations of the electrostatic free energy and internal energy changes in solution processes, *Chem. Phys.*, 1982, **65**, 239-245.

33. M. Cossi, V. Barone, R. Cammi and J. Tomasi, Ab initio study of solvated molecules: a new implementation of the polarizable continuum model, *Chem. Phys. Lett.*, 1996, **255**, 327-335.

34. V. Barone, M. Cossi and J. Tomasi, A new definition of cavities for the computation of solvation free energies by the polarizable continuum model, *J. Chem. Phys.*, 1997, **107**, 3210-3221.

35. E. Cancès, B. Mennucci and J. Tomasi, A new integral equation formalism for the polarizable continuum model: Theoretical background and applications to isotropic and anisotropic dielectrics, *J. Chem. Phys.*, 1997, **107**, 3032-3041.

36. B. Mennucci, E. Cancès and J. Tomasi, Evaluation of Solvent Effects in Isotropic and Anisotropic Dielectrics and in Ionic Solutions with a Unified Integral Equation Method: Theoretical Bases, Computational Implementation, and Numerical Applications, *J. Phys. Chem. B*, 1997, **101**, 10506-10517.

37. B. Mennucci and J. Tomasi, Continuum solvation models: A new approach to the problem of solute's charge distribution and cavity boundaries, *J. Chem. Phys.*, 1997, **106**, 5151-5158.
38. V. Barone and M. Cossi, Quantum Calculation of Molecular Energies and Energy Gradients in Solution by a Conductor Solvent Model, *J. Chem. Phys. A*, 1998, **102**, 1995-2001.
39. V. Barone, M. Cossi and J. Tomasi, Geometry optimization of molecular structures in solution by the polarizable continuum model, *J. Comput. Chem.*, 1998, **19**, 404-417.
40. M. Cossi, V. Barone, B. Mennucci and J. Tomasi, Ab initio study of ionic solutions by a polarizable continuum dielectric model, *Chem. Phys. Lett.*, 1998, **286**, 253-260.
41. R. Cammi, B. Mennucci and J. Tomasi, Second-Order Møller−Plesset Analytical Derivatives for the Polarizable Continuum Model Using the Relaxed Density Approach, *J. Chem. Phys. A*, 1999, **103**, 9100-9108.
42. M. Cossi, V. Barone and M. A. Robb, A direct procedure for the evaluation of solvent effects in MC-SCF calculations, *J. Chem. Phys.*, 1999, **111**, 5295-5302.
43. J. Tomasi, B. Mennucci and E. Cancès, The IEF version of the PCM solvation method: an overview of a new method addressed to study molecular solutes at the QM ab initio level, *J. Mol. Struct. Theochem*, 1999, **464**, 211-226.
44. R. Cammi, B. Mennucci and J. Tomasi, Fast Evaluation of Geometries and Properties of Excited Molecules in Solution: A Tamm-Dancoff Model with Application to 4-Dimethylaminobenzonitrile, *J. Chem. Phys. A*, 2000, **104**, 5631-5637.
45. M. Cossi and V. Barone, Solvent effect on vertical electronic transitions by the polarizable continuum model, *J. Chem. Phys.*, 2000, **112**, 2427-2435.
46. M. Cossi and V. Barone, Time-dependent density functional theory for molecules in liquid solutions, *J. Chem. Phys.*, 2001, **115**, 4708-4717.
47. M. Cossi, N. Rega, G. Scalmani and V. Barone, Polarizable dielectric model of solvation with inclusion of charge penetration effects, *J. Chem. Phys.*, 2001, **114**, 5691-5701.
48. M. Cossi, G. Scalmani, N. Rega and V. Barone, New developments in the polarizable continuum model for quantum mechanical and classical calculations on molecules in solution, *J. Chem. Phys.*, 2002, **117**, 43-54.

49. M. Cossi, N. Rega, G. Scalmani and V. Barone, Energies, structures, and electronic properties of molecules in solution with the C-PCM solvation model, *J. Comput. Chem.*, 2003, **24**, 669-681.

50. F. Lipparini, G. Scalmani, B. Mennucci, E. Cancès, M. Caricato and M. J. Frisch, A variational formulation of the polarizable continuum model, *J. Chem. Phys.*, 2010, **133**, 014106.

51. G. Scalmani and M. J. Frisch, Continuous surface charge polarizable continuum models of solvation. I. General formalism, *J. Chem. Phys.*, 2010, **132**, 114110.

52. T. H. D. Jr., Gaussian basis sets for use in correlated molecular calculations. I. The atoms boron through neon and hydrogen, *J. Chem. Phys.*, 1989, **90**, 1007-1023.

53. R. A. Kendall, T. H. D. Jr. and R. J. Harrison, Electron affinities of the first-row atoms revisited. Systematic basis sets and wave functions, *J. Chem. Phys.*, 1992, **96**, 6796-6806.

54. M. Head-Gordon, J. A. Pople and M. J. Frisch, MP2 energy evaluation by direct methods, *Chem. Phys. Lett.*, 1988, **153**, 503-506.

55. S. Sæbø and J. Almlöf, Avoiding the integral storage bottleneck in LCAO calculations of electron correlation, *Chem. Phys. Lett.*, 1989, **154**, 83-89.

56. M. J. Frisch, M. Head-Gordon and J. A. Pople, A direct MP2 gradient method, *Chem. Phys. Lett.*, 1990, **166**, 275-280.

57. M. J. Frisch, M. Head-Gordon and J. A. Pople, Semi-direct algorithms for the MP2 energy and gradient, *Chem. Phys. Lett.*, 1990, **166**, 281-289.

58. M. Head-Gordon and T. Head-Gordon, Analytic MP2 frequencies without fifth-order storage. Theory and application to bifurcated hydrogen bonds in the water hexamer, *Chem. Phys. Lett.*, 1994, **220**, 122-128.

59. S. Pari, I. A. Wang, H. Liu and B. M. Wong, Sulfate radical oxidation of aromatic contaminants: a detailed assessment of density functional theory and high-level quantum chemical methods, *Environmental Science: Processes & Impacts*, 2017, **19**, 395-404.

60. Z. A. Ali, F. W. Aquino and B. M. Wong, The diamine cation is not a chemical example where density functional theory fails, *Nature Communications*, 2018, **9**, 1-3.

61. J. B. Zheng, J. L.; Meana-Pañeda, R.; Zhang, S.; Lynch, B. J.; Corchado, J. C.; Chuang, Y.-Y.; Fast, P. L.; Hu, W.-P.; Liu, Y.-P.; Lynch, G. C.; Nguyen, K. A.; Jackels, C. F.; Fernandez Ramos, A.;Ellingson, B. A.; Melissas, V. S.; Villà, J. Rossi, I.; Coitiño, E. L.;

Pu, J.; Albu, T. V.; Ratkiewicz, A.; Steckler, R.; Garrett, B. C.; Isaacson, A. D.; Truhlar, D. G., *Polyrate*-version 2017-C, University of Minnesota, Minneapolis, 2017

62. J. B. Zheng, J. L.; Zhang, S.; Corchado, J. C.; Meana-Pañeda, R.; Chuang, Y.-Y.; Coitiño, E. L.; Ellingson, B. A.; Truhlar, D. G., Gaussrate 17, University of Minnesota, Minneapolis, 2017

63. Chemcraft - graphical software for visualization of quantum chemistry computations, https://www.chemcraftprog.com).

64. M. E. Bender, The toxicity of the hydrolysis and breakdown products of malathion to the fathead minnow (Pimephales Promelas, Rafinesque), *Water Res.*, 1969, **3**, 571-582.

65. C. J. Miles and S. Takashima, Fate of malathion andO,O,S-trimethyl phosphorothioate by-product in Hawaiian soil and water, *Arch. Environ. Contam. Toxicol.*, 1991, **20**, 325-329.